Fuzzy c-means approach to tissue classification in multimodal medical imaging

S. Banerjee *, D.P. Mukherjee, D. Dutta Majumdar

Electronics and Communications Sciences Unit, Indian Statistical Institute, 203 Barrackpore Trunk Road, Calcutta 700035, India

Received 1 January 1997; accepted 29 December 1997

Communicated by Azriel Rosenfeld

Abstract

A fuzzy c-means approach is described for tissue segmentation of X-ray computed tomography (CT) and T1 weighted magnetic resonance (MR) images of the same cross-section of the human brain. A fuzzy set approach is then utilized to obtain a fused classification displaying the salient features of image data of the individual modalities.

Keywords: Segmentation; Data fusion; Multimodality imaging; Fuzzy c-means

1. Introduction

In recent times, rapid technological advances have led to the creation of a number of sensors that can image different phenomena in the object to be imaged, from different points of view. Each individual sensor relies on a particular physical property of the object to produce a 2D image (on pixels) or a 3D image (on voxels). Thus, the strength/weakness of a particular sensor depends on its ability to pick up a variation of signals it receives from the entire volume of the object to be imaged as well as the resolution. Hence, in medical applications, for instance, integration of images from different modalities

would offer the physician with better diagnostic capabilities and an improvement in surgical and therapy planning and evaluation. Intelligent diagnostic systems such as machine vision platforms are designed to combine and display the salient features of individual modalities on a single platform, in an attempt to accomplish this purpose. Such systems always include algorithms like segmentation, registration and data fusion.

Several techniques have been attempted to segment medical images. These include Bayesian maximum likelihood [1] ANN [2], Dempster-Shafer evidential reasoning in magnetic resonance (MR) and computed tomography (CT) images [3], a 3D extension of the Marr-Hildreth operator in MR [4] images and use of low-level features in MR [5] images among others. Hall et al. [6] utilized the fuzzy c-means algorithm developed by Bezdek [7] for MR images. The fuzzy c-means clustering approach can be described as a fuzzy, serial, unsupervised pixel classification technique based on iterative approximation of local minima to global objective functions. A variation of fuzzy c-means has also been used to estimate CSF and image matter volumes [8]. This algorithm has two advantages, namely its robustness to noise and its being an unsupervised algorithm. We extend method of Hall et al. [6] to MR and CT image segmentation and use these segmented images to obtain a fused classification as multimodal images offer better segmentation results than those from a single modality. Previous attempts to segment CT and MR images have been described by the authors [9]. It is difficult to assess the quality of segmentation quantitatively and generally this done by visual inspection and confirmation from a domain expert (e.g. a radiologist).

When images of the same cross-section of the human head obtained from two modalities are being combined, image registration can be performed using a small number of equivalent features such as points or surfaces in the images [10–13]. These methods employ a small number of derived features of the images and point matching techniques yield more accurate results only for regions surrounding the landmarks. On the other hand, if a number of voxels corresponding to an ROI in one image can be registered with the same ROI of another image results are bound to be more accurate than those obtained with a few points, as such a method is likely to be more robust to noise and less prone to truncation effects caused by the partial overlap of imaged volumes. This forms the basis of our registration scheme.

Fusion of image data from different sensors succeeds registration. Generally, the images to be combined in data fusion problems [14] are partly redundant as the same ROI are depicted in all the images, and also partly complementary as each modality highlights certain features which are distinctive from the other sensors. As mentioned earlier, no individual modality is complete and, furthermore, some of the information provided is likely to be imprecise and uncertain. The integration of the salient features of images produced by different modalities serves the twofold purpose of increasing the global information

while reducing the imprecision and uncertainty pertaining to a single sensor. Present day data fusion methods mostly utilize high level information extracted from preprocessing steps, with the help of rule-based systems. When direct global decisions are not possible, as in situations involving numerical information and its imperfections, local decisions are combined to form global decisions. Such numerical methods are generally used for pixel based fusion used in image classification [15]. To date, probabilistic fusion and Bayesian inference are the widely used approaches to data fusion. Alternate approaches include the Dempster-Shafer evidence theory [14], possibility theory and fuzzy sets theory. We use an adaptation of fuzzy sets theory in our endeavors to obtain a fused classification.

In this paper we propose an algorithm which uses the fuzzy c-means approach to segment same cross-sections of CT and MR images of the brain of a patient. This is a pixel based approach to segmentation. The histograms of the observed pixel intensities are studied with a view to obtain thresholds for tissue classification. It is a semi-automated classification scheme where the operator identifies seed pixel locations for each of the tissue classes and the fuzzy c-means clustering algorithm assigns labels to the remaining pixels. Registration of the images is performed using a correlation type scheme. Fusion of the images for displaying the complementary and redundant features is then performed.

The main advantages of this technique are its computational simplicity and robustness to noise. In addition, this technique is less prone to truncation effects and is an unsupervised training method. Since this is a semiautomated approach, it can be adapted to a variety of multimodality imaging methods. In addition to ideal situations, this method can be used when one of the sensors can depict some classes clearly while others cannot and global knowledge of the reliability of the individual sensors can also be utilized.

In the next section, a brief outline of the fuzzy c-means clustering is given. In Section 3, the application of this algorithm to the segmentation of MR and CT images is detailed. Section 4 contains an example of CT and MR image fusion of Figs. 1 and 2 followed by concluding remarks in Section 5.

2. The algorithm

Following Hall et al. [6], we use the fuzzy c-means algorithm to perform to perform segmentation of cross-sections of the human brain from the two modalities CT and MR. This image segmentation technique can be classified as a pixel classification scheme. Each pixel is classified according to its grey value in each of the images of the two modalities. This algorithm has two advantages over other methods. First, classification is performed without prior training, and second, the method is robust to missing and noisy data.

The c-means (CM) algorithm takes a finite data set $\mathbf{X} = (x_1, x_2, \ldots, x_n)$ in R^p as its input with each $x_j \in \mathbf{X}$ being a feature vector. $x_j = (x_{j1}, x_{j2}, \ldots, x_{jn})$ where x_{ij} is the jth feature of subject x_i. The function u, a fuzzy subset of **X**, is defined as follows

$u_i : \mathbf{X} \Rightarrow [0, 1]$ assigns to each x_i in **X** its grade of membership in the fuzzy set U. In order to partition **X** by means of fuzzy sets, a fuzzy c-partition is defined as a $c \times n$ matrix U such that:

(1) Each row U_i is the ith fuzzy subset of **X**.

(2) Each column U_j exhibits the membership grades of datum j in every fuzzy subset.

(3) The sum of membership grades of each datum in all of the fuzzy subsets, is unity.

(4) There is no empty fuzzy subset.

(5) No fuzzy subset is all of **X**.

The fuzzy c-means functional can be written [10] in the fuzzy c-prototypes form (for $1 < c < n$)

$$J_m(U, v; X) = \sum_{i=1}^{c} \sum_{k=1}^{n} (u_{ik})^m D_{ik}, \tag{1}$$

where $m \in [1, \inf]$ is a weighting exponent on each fuzzy membership, $U \in M_f$ is a fuzzy c-partition of **X**, $v = (v_1, v_2, \ldots, v_c)$ are (geometric) cluster prototypes, $v_i \in R^p$, D_{ik} is some measure of similarity, (like error or proximity) between v_i and x_k. $D_{ik} = \|x_k - v_i\|_A^2$. A is positive definite. $\|x\|_A^2 = x^{\mathrm{T}} A x$. J_m is thus iteratively minimized.

The steps involved in the algorithm are as follows.

(1) Fix the number of clusters c.

(2) Start with some initial matrix U.

(3) Compute the new cluster centers v_i as a function of the input vectors x_j and the membership grades u_{ij}.

(4) Update U using D_{ik}^2.

(5) If the difference between the new U and previous U is less than a preset tolerance limit, then STOP, else go back to step 3.

For greater accuracy, we use two statistical features, average and busyness, instead of pixel values of T1, T2 and PD weighted images used in Ref. [6]. These are defined as follows.

2.1. Feature vectors

Since, we have no a priori information about the cluster seed points, image texture or grey value distribution, we have selected feature vectors such that they represent the closest possible nature or homogeneity of any image subregion. Using standard masking techniques of image processing, for the subimage.

m_{00}	m_{01}	m_{02}
m_{10}	m_{11}	m_{12}
m_{20}	m_{21}	m_{22}

the following feature vectors are calculated for m_{11}.

1. The average grey values (aver) of m_{11}, aver $(m_{11}) = 1/9 \sum_{i=0,j=0}^{2,2} m_{ij}$.

2. The busyness value (buz) of m_{11}, buz $(m_{11}) = \min(\text{buz}_h, \text{buz}_v)$ where, $\text{buz}_h = \sum_{i=0}^{2} |m_{i0} - m_{i1}| + |m_{i1} - m_{i2}|$ and $\text{buz}_v = \sum_{j=0}^{2} |m_{0j} - m_{1j}| + |m_{1j} - m_{2j}|$. The busyness value is influenced by the (horizontal or vertical) orientation of grey value distribution.

3. Segmentation

Tissues that are of interest in brain image segmentation include the skull, brain matter (consisting of gray and white matter), ventricles (V), and extra-ventricular cerebrospinal fluid (CSF), fatty tissue and any abnormal region(s) comprising of pathologies. Data used in this study correspond to CT and MR images. The skull and other hard tissues, CSF and V can be detected in CT images. CSF and V are also easy to detect in MR images. Segmentation of the brain matter into white (WM) and grey matter (GM) is generally difficult, although the distinctions are better in MR images than in CT images.

Therefore, a fused image cross-section which depicts the hard tissues obtained from CT and soft tissues from MR would provide more complete information than any individual modality alone (e.g. CT or MR). V and CSF show up in both images and these redundancy features in both images are used to register the images before fusing the highlights of the individual images.

Fig. 1 is an MR image (242 × 242 pixels) section of the brain which clearly depicts the ventricle (V) and CSF. However, the WM and GM cannot be so clearly distinguished although these are more distinct in the MR image than the CT image (Fig. 2), which is a CT image (256 × 256 pixels) of the same cross-section. In the CT image, the skull is more clearly depicted and V and CSF can also be seen.

Fig. 1(a) and (b) are, respectively, the T1 weighted MR (original image is 242 × 242 pixels, TR = 400 ms, TE = 12 ms) and CT (256 × 256) image of the same region of the brain of a normal human subject. Fuzzy c-means is an unsupervised segmentation scheme, and so it is applied directly to the image. The matrix U defined in Section 2 is converted to a hard c-partition by assigning each pixel to the tissue class with maximum membership value, in order to use it for segmentation. Two features, average and busyness, are considered for each pixel. Thus, for each of the images (Fig. 1(a) and (b)) the input to the FCM is a

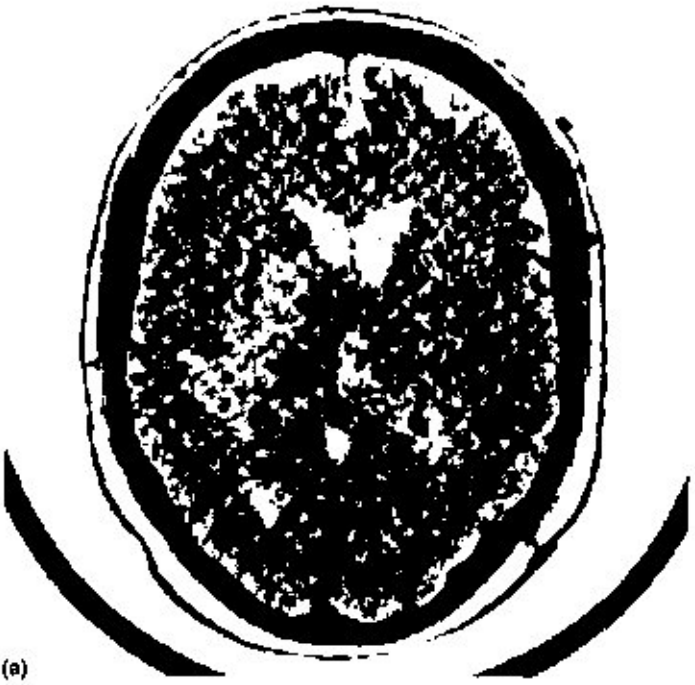

(a)

(b)

Fig. 1. (b) represents original MR image and Fig. 1(a) represents original CT image (CT images reverse videographed to represent skull clearly) of same region of brain of normal subject.

65 536 × 2 matrix. The Euclidian inner product norm was used to compute the similarity measure D_{ik}. FCM was run for each image using 15 iterations for 3–6 classes. Fig. 2(a) and (b) represents another set of MR and CT images.

Evaluation of the results of segmentation was done by visual inspection and comparison with raw images, and also confirmed by a radiologist. Based on this evaluation, four clusters were found to be optimum for segmentation of MR and five clusters were best for CT. These clusters corresponded to air, CSF, brain (WM and GM) matter and fatty tissue for MR and air, CSF, brain matter (WM and GM), fatty tissue and skull for CT. Due to the inherently better resolution of MR as compared to CT, MR images yielded better segmentation results. This is also consolidated by the graphs of grey levels versus number of pixels (excluding background noise), shown in Fig. 3(a) and (b) for MR and CT, respectively where the peaks are more prominent for MR. Segmented images for four and five clusters of image set of Fig. 1 are shown in Fig. 5(a) and (b) for MR and CT, respectively and for the other clusters are given in Fig. 4(a) and (b). Final segmented images of the second image set (Fig. 2) are given in Fig. 6c(a) and (b).

Table 1 lists the cluster centers corresponding to the average and busyness vectors for MR and CT, respectively, and Table 2 gives an Euclidian distance between the corresponding cluster centers of the two images. This Euclidian distance is

$$d_{\mathrm{st}} = \sqrt{(\mathrm{aver_M} - \mathrm{aver_C})^2 + (\mathrm{buz_M} - \mathrm{buz_M} - \mathrm{buz_C})^2}, \tag{2}$$

where aver denotes average and buz denotes busyness and the subscripts M and C correspond to MR and CT, respectively.

The last column of Table 2 gives the MR cluster center which best matches the CT cluster given in the first column. Based on grey level value (0–255) considerations, the first cluster (lowest grey value) center corresponds to air. The second cluster center corresponds to CSF while the third cluster center corresponds to brain matter (WM and GM) and fourth fatty tissue in MR and CT. From an inspection of Figs. 1(a) and 2(a), and the corresponding graph (Fig. 3(a)), we find that the fifth cluster center corresponds to the skull region for CT. This classification also follows from Hounsfield number considerations in CT and proton signal intensity considerations in MR. An inspection of Table 2 reveals that, based on the Euclidian measure of similarity, matches were good for all tissues of interest other than fatty tissue.

4. Data fusion

Data fusion involves the combination of information from several different sources to obtain a more complete picture than that which would be available

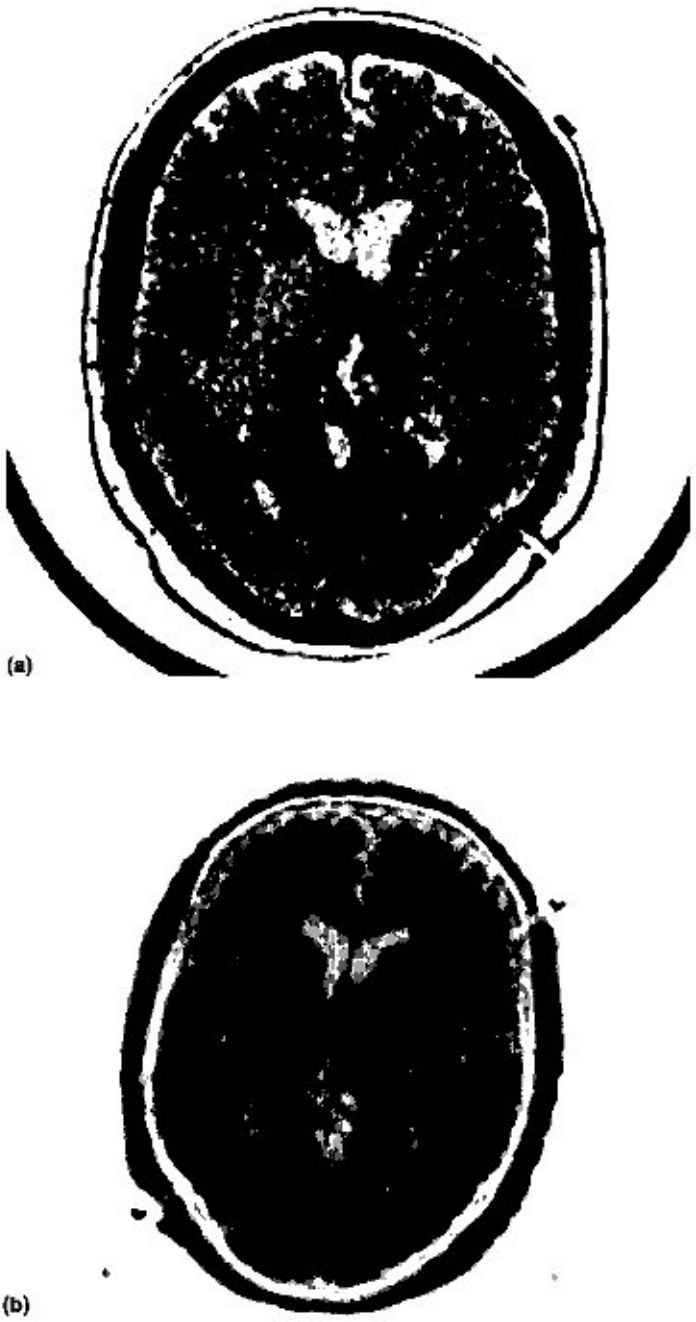

Fig. 2. (b) and (a) represents a second set of MR and CT images of the same subject.

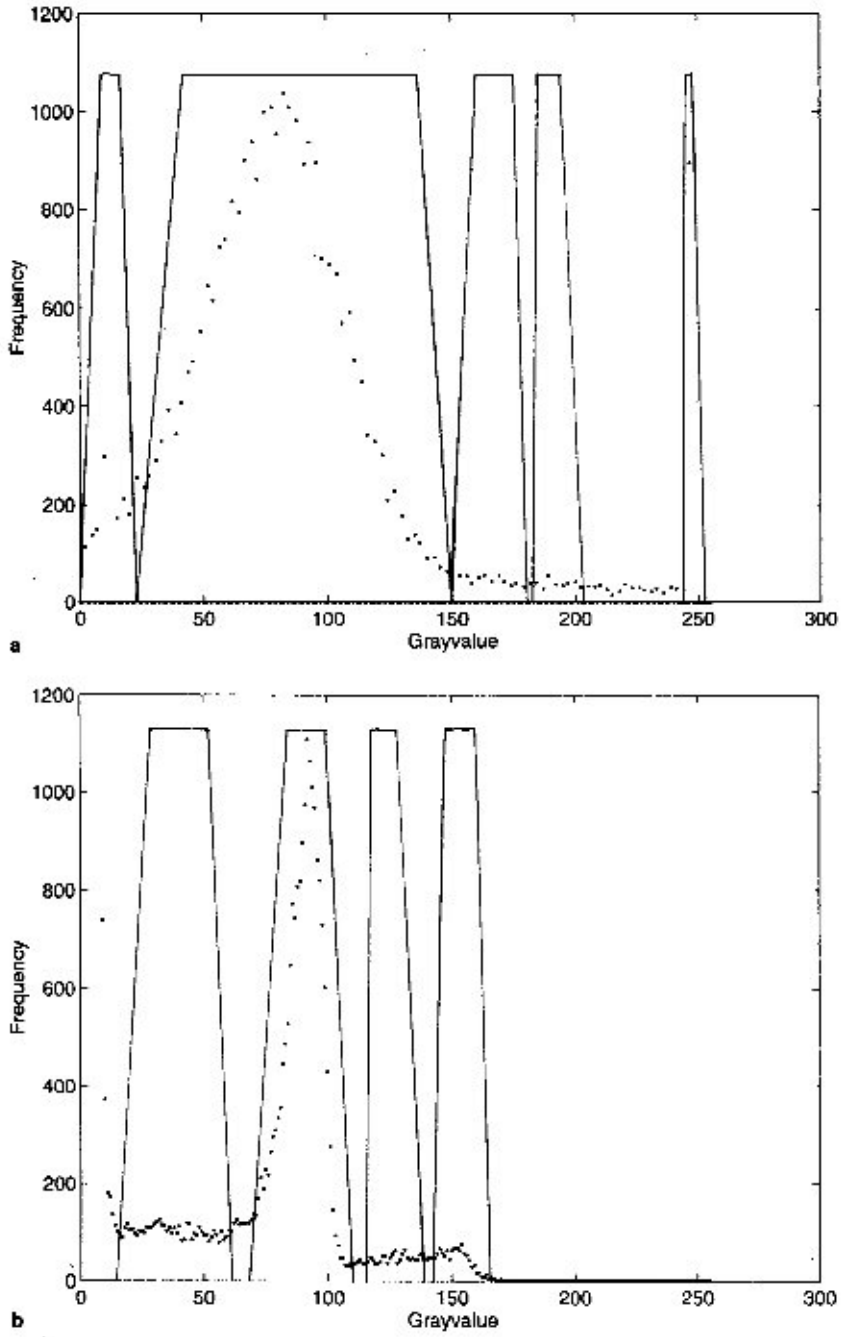

Fig. 3. (b) and (a) represent MR and CT image histograms, respectively, corresponding to the image set of Fig. 1.

from a single source. Thus, data fusion can involve a combination of signals from different sensors for the same field of view, or a combination of signals from different media or a combination of signals obtained from a given sensor obtained from different fields of view. In our application, we consider signals from two different sensors MR and CT, imaging the same region of the human brain. This information obtained from the different sensors which can be either

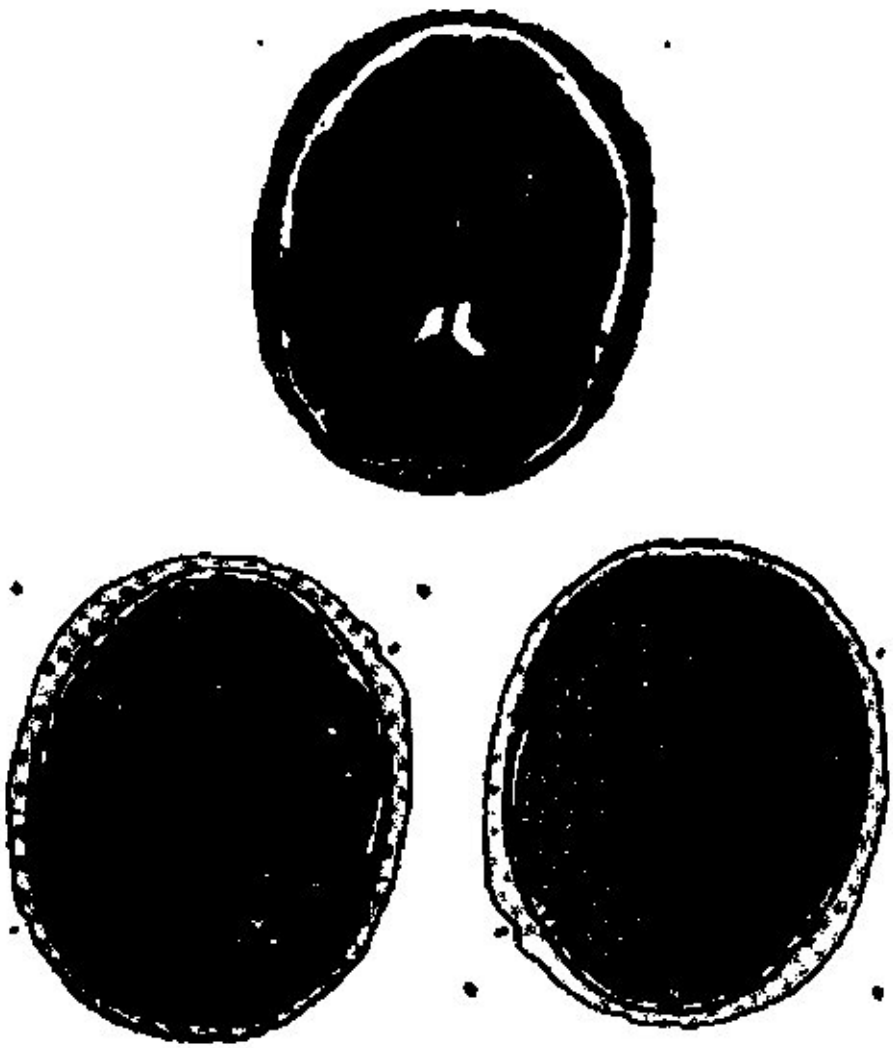

Fig. 4. (a) and (b) represents MR and CT images segmented with different clusters. Fig. 4(a) shows 3, 5 and 6 clusters for MR and 3, 4 and 6 clusters for CT.

Fig. 4b (continued).

symbolic or numeric, is given by degrees of belief in an event and accounts for the imprecision, uncertainty and incompleteness of the information from each sensor. Numerical fusion operators combine these degrees of belief. Three classes of such operators have been defined in Ref. [16]. In our classification problem, we use the third class, namely, the Context Dependent (CD) data fusion operator. This operator depends on the two variables representing the degrees of the sources of information to be combined, as well as a global knowledge or measure on these sources. This measure can be conflict between the sources, or a reliability between them or a mutual compromise.

In this section, we describe our attempts to design CD data fusion operators for classification problems in multimodal medical imaging, and CT and MR images of the brain, in particular. Considerations that we have taken into

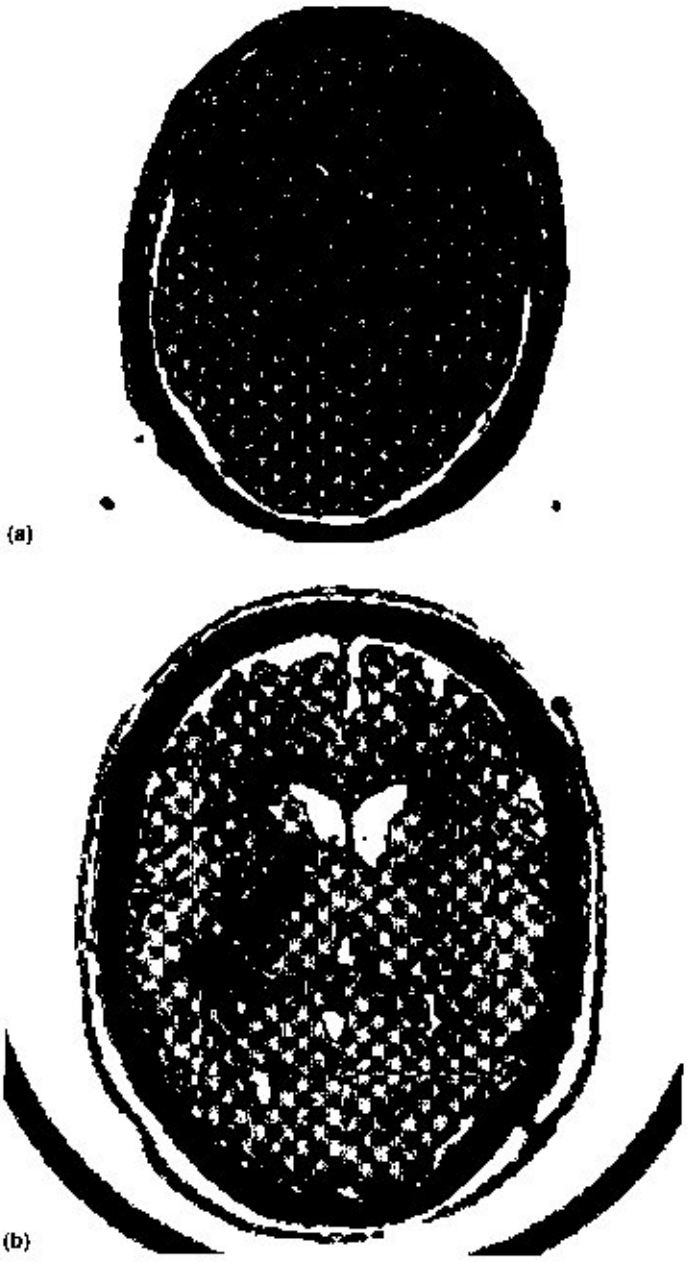

Fig. 5. (a) represents MR image segmented into four classes and (b) represents CT image segmented into five classes, for image set of Fig. 1.

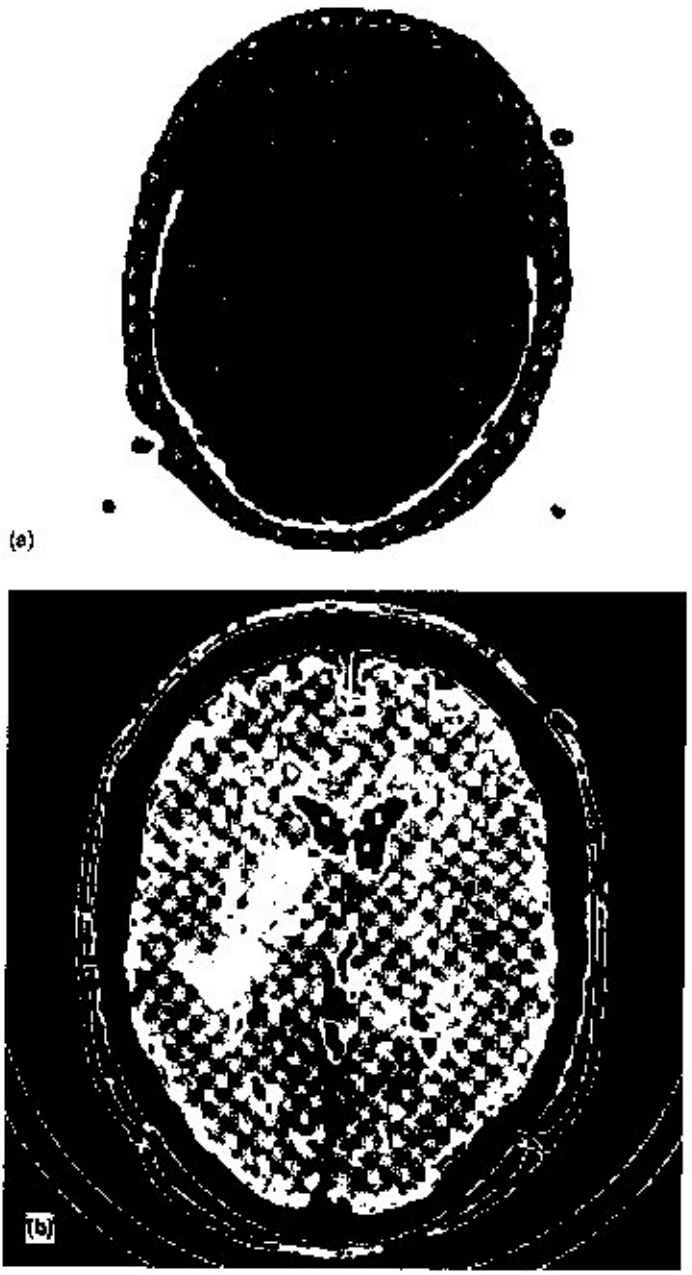

Fig. 6. (a) and (b) represents segmented MR (4 classes) and CT (5 classes) images corresponding to Fig. 2.

Table 1
Cluster centers for the CT and MR images of Figs. 1 and 2

Figure	Modality	Cluster centers		Class name
		Average	Busyness	
1(b)	CT	1.041	0.824	Air
		89.766	13.853	Brain matter
		57.135	17.177	CSF
		158.955	58.474	Fat tissue
		244.343	2.303	Skull
1(a)	MR	4.747	0.714	Air
		85.805	3.754	Brain matter
		100.828	4.212	Fat tissue
		45.755	12.508	CSF
2(b)	CT	51.096	18.340	CSF
		83.592	13.263	Brain matter
		0.809	0.651	Air
		122.440	37.946	Fat tissue
		242.409	3.955	Skull
2(a)	MR	4.706	0.756	Air
		85.093	3.635	Brain matter
		100.498	4.428	Fat tissue
		45.462	12.162	CSF

Table 2
Computation of d_{ks}

Figure	MR	1	2	3	4	Conclusion
	CT (1–4)					
1	1	3.71	84.8	99.8	46.2	Matches MR (1)
	2	86.1	11.7	14.7	44.0	Matches MR (2)
	3	54.9	31.7	45.6	12.3	Matches MR (4)
	4	164.7	91.4	79.5	122.2	Matches MR (3)*
2	1	49.6	37.0	51.3	8.36	Matches MR (4)
	2	78.9	9.74	19.06	38.2	Matches MR (2)
	3	3.90	84.3	84.3	99.8	Matches MR (1)
	4	123.5	50.7	46.1	81.9	Matches MR (3)*

* Most preferred modality.

account in our design of CD operators include global reliability of the different sensors for imaging a particular anatomical region of a human subject as well as the behavior of these sensors towards each of the tissue classes comprising the organ. We use the morphological images of the brain of a human subject from CT and MR sensors of Fig. 1, as an example. Global reliability of CT and MR for morphological images of the brain are well acknowledged as is the global reliability of Positron Emission Tomography (PET)/Single Photon Emission Computed Tomography (SPECT) for functional imaging of the brain. In morphological images, bony tissues and classification are not at all well imaged by MR owing to the poor proton signals obtained. On the other hand, CT is found to be most reliable for bony tissues. In CT images, the Hounsfield number for bone is 1000, calcified tissue is 80, grey matter lies between 36–46, white matter between 22–32, water is 0 and air is −1000 [17]. This indicates that grey matter and white matter lie close to each other and are difficult to distinguish in CT images. Grey and white matter signals are also close to each other in T1 weighted MR images. However, MR is the preferred modality for imaging soft tissues. These remarks are summarized in Table 3. Our objective is to obtain a fused classification of these tissue types based on the global reliability of CT and MR for these individual sources as well as the degrees of belief of these sources for each tissue type.

Let D denote the two dimensional integer lattice consisting of pixels which contain the fused image. D contains five tissue classes of interest, air, WM, GM, V and CSF and skull. Simple hypotheses in D are considered. Membership functions in these classes are simple probabilities deduced from the frequencies obtained from the histogram (which are normalized). The original resolution of the CT image (256 × 242) is reduced to (242 × 242) by a factor of 1.057 to the MR resolution.

Images registered using a pixel based correlation scheme are fused using an image fusion operator. This image fusion operator can be defined in the form of a blending function F defined as follows.

Table 3
Source reliability for individual tissue types

Tissue type	Source	
	CT	MR
Air	Poor	Better than CT
V and CSF	Good	Good (better than CT)
Brain matter	Good	Good (better than CT)
Skull	Excellent[a]	Poor

[a] Most preferred modality.

$$F = k * I_1 + (1 - k) * I_2, \tag{3}$$

where I_1 and I_2 are the segmented portions from modalities 1 and 2 to be fused and k is the degree of fusion depending on the membership function of these modalities to the individual classes and the degree of conflict between the sources. This degree of conflict is obtained from the Euclidian distances for the two matched classes obtained from Table 2. This distance is ideally zero for the matched class and thus the sources are consonant and so the fusion operator is conjunctive. The sources are dissonant for the tissue class 'skull', so the operator is disjunctive and favors the CT modality.

From Table 2 it is found that, for matched classes, the Euclidian distance is minimum though not actually zero. So there is a partial conflict and a compromise is made in the choice of k. k is taken to be the sum of the difference in membership values and degree of conflict (as given by the Euclidian distance) and considered as the percentage of deviation from the case when both images are equally blended. The sign of the difference of membership values are taken from global reliability. The reason for using this expression for k is to take into account the maximum deviation from uniform blending resulting out of the conflict of the two sensors and misclassification of one of the sensors assuming that the other sensor is more reliable. So, for the ith class,

$$k_i = (m_i^1 + m_i^2 \cdot \text{conflict}(m_i^1, m_i^2)) + 0.5, \tag{4}$$

where m_i^j represents the membership of image data of the first sensor (CT) and superscript 2 is for the second sensor (MR). Values of k for the different classes are given in Table 4 for Figs. 1(b) and 2(b).

This data fusion operator is usable for weak coupling when the contribution from one modality is predominant and for strong coupling when both modalities contribute substantially. With these considerations, we obtain the fused classification shown in Fig. 7(a) and (b) for image sets Figs. 1 and 2. Results of the fused displays indicate that the major tissue classes of MR, namely, brain matter, CSF and fatty tissue have been highlighted along with the major classes

Table 4
Values of k

Tissue type	k (Fig. 1b)	k (Fig. 2b)
Air	0.46	0.40
V and CSF	0.38	0.30
Brain matter	0.38	0.30
Fat tissue	0	0
Skull	1.0	1.0

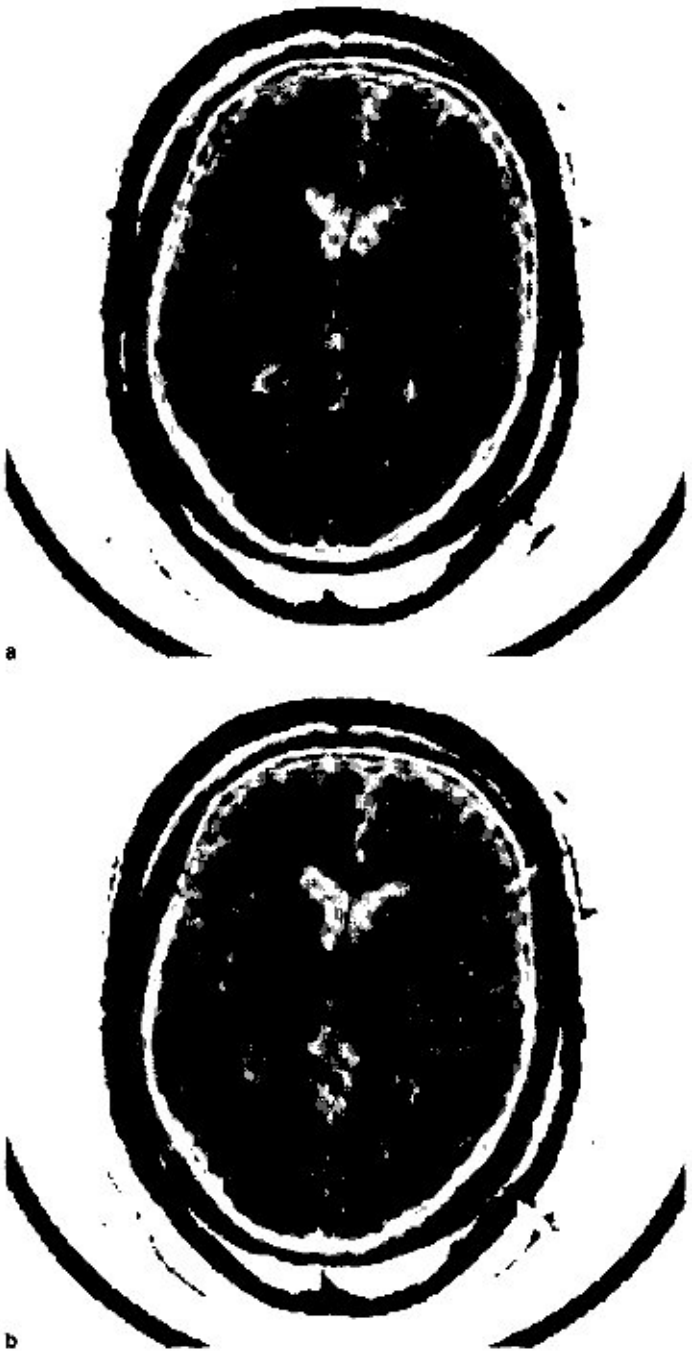

Fig. 7. (a) and (b) represents the fused (MR and CT) classification for images of Figs. 1 and 2.

of CT, which is the skull. Some inaccuracies in the overlay are due to the fact that although the original images are of the same region of the human subject, they are not absolutely identical due to the inherently different imaging procedures involved. It is also hoped that with an improvement of correlation based registration technique, which is still an open field of research, blending will be more accurate.

We have considered hard membership to each class as we have designed the membership functions as simple trapezoidal forms with a negligibly small degree of overlap (see Fig. 3(a) and (b)). Fuzzy memberships can also be considered in cases where there is a substantial degree of overlap. For the design of such membership functions, see Ref. [18].

5. Concluding remarks

We have presented the results of segmentation of CT and MR images of the same region of the brain of a patient using the fuzzy CM algorithm which is an unsupervised algorithm, robust to noise and computationally very simple. It was found that for normal tissues, MR (T1) shows best results when four classes are used whereas CT gives best results for five classes.

A data fusion operator which obtains a fused classification from these two images is defined. This fusion operator combines the segmented portions of the two images after registration, depending upon their membership function to the class and the degree of conflict obtained from the Euclidian measure of dissimilarity. Hard memberships in these classes are considered as the class partitions are well defined, though fuzzy memberships could also be used for fuzzy partitions.

The scheme described in this paper for fused classification is computationally simple and can be applied to ideal cases as well as when the source provides information about only a few of the several sensor classes to be fused. It can also be used when a sensor differentiates two classes when others may not and incorporates information regarding global source reliability. Mixed pixel effects can be incorporated using fuzzy membership schemes. Since this is a semi-automated approach to data fusion, it offers a strong advantage in terms of flexibility. With some knowledge of anatomy, it is hoped that one can obtain fused images for different modalities, e.g., dual echo MR images, functional and morphological images and images acquired at different times, as well as images of different parts of the human body. The domain expert can utilize such a scheme to suit a particular need. Trials of this technique to images of different organs with and without pathology, taken at different times and with different modalities provide scope for further research. This technique also offers possibilities to other application domains of image processing like remote sensing.

Acknowledgements

This work is partially supported by Department of Science and Technology, Government of India. We would like to thank Drs. J.M. Rocchisani and O. Monga of INRIA, France, for kindly providing image data. We would also like to thank Dr. A. Bhargava of JMD Medicare, Calcutta for his assistance in interpreting the images.

References

[1] M.W. Vannier, C.M. Speidel, D.L. Rickman, Magnetic resonance imaging multispectral tissue classification, NIPS, vol. 3, Aug. 1991.
[2] L.P. Clarke et al., Comparison of supervised pattern recognition techniques and unsupervised methods for MRI segmentation, Medical Imaging IV, Newport Beach, CA, Feb. 1992.
[3] S. Chen, L. Wei-chun, C. Chen, Medical image understanding system based on Dempster-Shafer reasoning, SPIE Biomedical Image processing II, San Jose, CA, 1991.
[4] M. Bomans, K.H. Hohne, U. Tiede, M. Riemer, 3D segmentation of MR images of the head for 3D display, IEEE Trans. Medical Imaging 9 (2) (1990).
[5] S.P. Raya, Low-level segmentation of 3D magnetic resonance images-A rule based system, IEEE Trans. Med. Imaging 9 (3) (1990).
[6] L.O. Hall, A.M. Bensaid, L.P. Clarke, R.P. Velthuizen, M.S. Silbiger, J.C. Bezdek, A comparison of Neutral Network and Fuzzy Clustering Techniques in Segmentation of MR images of the Brain, IEEE Trans. Neural Networks 3 (5) (1992).
[7] J. Bezdek, Pattern Recognition with Fuzzy Objective Function Algorithms, Plenum Press, New York, 1991.
[8] M.E. Brandt, T.P. Bohan, L.A. Kramer, J.M. Fletcher, EStimation of CSF, white and grey matter volumes in hydrocephalic children using fuzzy clustering of MR images, Comput. Medical Imaging Graphics 18 (1994) 25–34.
[9] S. Banerjee, D. Dutta Majumdar, S. Kobh, V. Mishra, Tissue Classification using Multimodal Medical Imaging, Proc. Comput. Assist. Radiol. (CAR'96), Paris 1996, p. 1005.
[10] S. Banerjee, D.P. Mukherjee, D. Dutta Majumdar, Point Landmarks for the registration of CT and MR images, Patt. Recog. Lett. 16 (1995) 1033–1042.
[11] D.L.G. Hill, D.J. Hawkes, J.E. Crossman, M.J. Gleeson, T.C.S. Cox, E.E.C.M.L. Bracey, A.J. Strong, P. Graves, Registration of MR and CT images for skull base surgery using point like anatomical features, Br. J. Rad. 64 (1991) 1030–1035.
[12] C.A. Pelizzari, G.T.Y. Chen, D.R. Spelbring, R.R. Weichselbaum, C.T. Chen, Accurate 3D registration of CT, PET and/or MR images of the brain, J. Comput. Assist. Tomogr. 13 (1989) 20–26.
[13] H. Jiang, R.A. Robb, K.S. Holton, New Approach to 3D registration of multimodality medical images by surface matching, Visualization in Biomedical Computing, Proc. Soc. Phot.- Opt. Instrum. Eng. 1808 (1992) 196–213.
[14] I. Bloch, Some aspects of Dempster-Shafer evidence theory for classification of multimodality medical imaging taken partial volume effects into account, Patt. Recog. Lett. 17 (1996) 905–919.
[15] I. Bloch, H. Maitre, Fusion de donnees en traitement d'images: Modeles d'information et decisions, Traitement du signal 11 (1994) 435–446.
[16] I. Bloch, Information combination operators for Data Fusion: A Review with classification, IEEE Trans. Syst., Man Cybernet. Part A: Systems and Humans 26 (1996) 52–67.
[17] D. Sutton, A Textbook of Medical Imaging, Churchill Livingston, London, 1984.
[18] J.T. Kent, K.V. Mardia, Spatial classification using fuzzy membership, IEEE Trans. Patt. Anal. Mach. Intell. PAMI-10 (1988) 659–671.